Earth Surface Processes and Landforms
Earth Surf. Process. Landforms **32**, 1491–1502 (2007)
Published online 16 February 2007 in Wiley InterScience
(www.interscience.wiley.com) **DOI:** 10.1002/esp.1472

GIS-assisted modelling for debris flow hazard assessment based on the events of May 1998 in the area of Sarno, Southern Italy: Part I. Maximum run-out

G. Toyos,[1]* D. Oramas Dorta,[2] C. Oppenheimer,[1] M. T. Pareschi,[3] R. Sulpizio[4] and G. Zanchetta[5]

[1] *Department of Geography, University of Cambridge, Cambridge, UK*
[2] *Department of Geography, Coventry University, Coventry, UK*
[3] *Istituto Nazionale di Geofisica e Vulcanologia (INGV), Pisa, Italy*
[4] *Dipartimento Geomineralogico, Universita di Bari, Bari, Italy*
[5] *Dipartimento di Scienze della Terra, Universita di Pisa, Pisa, Italy*

**Correspondence to: Dr. Guillermo Toyos, Comisión Nacional de Actividades Espaciales (CONAE), Av. Paseo Colón 751, 1063 Buenos Aires, Argentina. E-mail: gtoyos@conae.gov.ar*

Received 23 December 2005;
Revised 1 November 2006;
Accepted 8 November 2006

Abstract

Based on the debris flow events that occurred in May 1998 in the area of Sarno, Southern Italy, this paper presents an approach to simulate debris flow maximum run-out. On the basis of the flow source areas and an average thickness of 1·2 m of the scarps, we estimated debris flow volumes of the order of 10^4 and 10^5 m^3. Flow mobility ratios ($\Delta H/L$) derived from the x, y, z coordinates of the lower-most limit of the source areas (i.e. apex of the alluvial fan) and the distal limit of the flows ranged between 0·27 and 0·09. We performed regression analyses that showed a good correlation between the estimated flow volumes and mobility ratios. This paper presents a methodology for predicting maximum run-out of future debris flow events, based on the developed empirical relationship. We implemented the equation that resulted from the calibration as a set of GIS macros written in Visual Basic for Applications (VBA) and running within ArcGIS. We carried out sensitivity analyses and observed that hazard mapping with this methodology should attempt to delineate hazard zones with a minimum horizontal resolution of 0·4 km. The developed procedure enables the rapid delineation of debris flow maximum extent within reasonable levels of uncertainty, it incorporates sensitivities and it facilitates hazard assessments via graphic user interfaces and with modest computing resources.

Keywords: debris flows; volume; mobility; GIS; hazard assessment

Introduction

Debris flows are fully saturated mixtures of water and sediment (Iverson, 1997) that can travel tens of kilometres from the source areas, representing a serious hazard to society (Iverson *et al.*, 1998; Pierson, 1995). They are common on volcano slopes, where they may occur during or after an eruption. Volcanic debris flows are also known as 'lahars' (Smith and Lowe, 1991). Similarly, mountainous areas mantled by volcanic deposits from explosive eruptions are prone to the occurrence of debris flows triggered by heavy rainfall, which represent a permanent hazard for the people and infrastructure downslope. This is the case of the Sarno Mountains, located eastwards from Mt. Somma–Vesuvius (Southern Italy) (Figure 1), and was tragically demonstrated in May 1998, whereby after two days of very intense rains the upper slopes collapsed and evolved into debris flows that affected the areas of Episcopio, Lavorate, Quindici, Siano and Bracigliano (Figure 1) (Calcaterra *et al.*, 2000; Pareschi *et al.*, 2000; Zanchetta *et al.*, 2004) and the Clanio valley (Pareschi *et al.*, 2002). As a result, more than 150 people were killed and there was substantial damage to property (Calcaterra *et al.*, 2000; Porfido *et al.*, 2002; Pareschi *et al.*, 2000; Toyos *et al.*, 2003). Thus, hazard assessments and planning for the reduction of risk should be a priority of the public administration and civil protection authorities in areas that could be affected by debris flows. In this context, the development of methods for identifying areas potentially endangered by debris flows constitutes a critical issue for the scientific community.

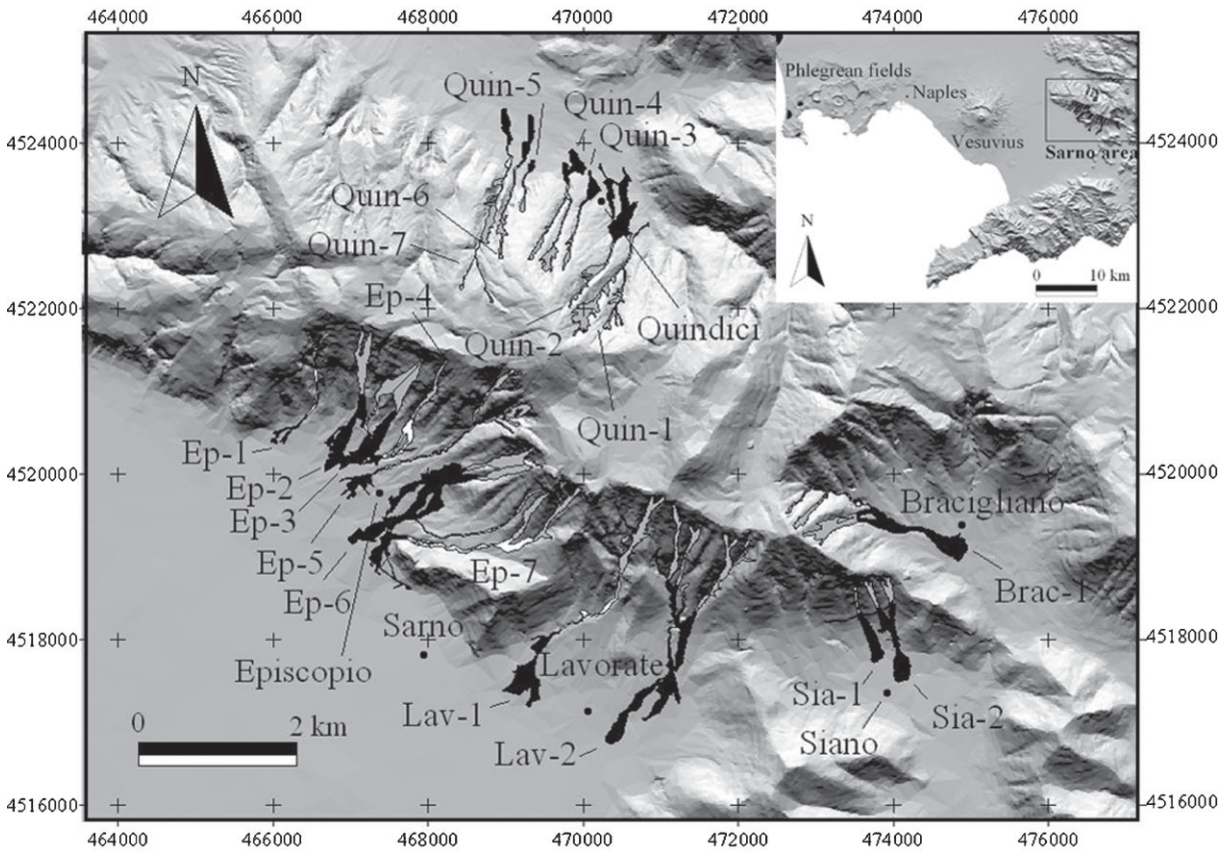

Figure 1. Shaded relief map of the Sarno area and the regional setting (inset). The May 1998 debris flows are shown. Grey indicates the source areas, white, the transport zones and black, the deposition areas. When inundation areas could not be resolved the two or more flows were assumed as a single event, i.e. the volumes of the corresponding source areas were added accordingly (e.g. Lav-2 with four source areas.). The labels in these cases indicate the assumed single event and not the single source areas originally identified (e.g. Lav-2a to Lav-2d, see Table I). The projection of the map is UTM, European Datum 1950 (the units of the grid are in metres).

Debris flow hazard mapping may involve the use of geological and geomorphological observations and historical data and the application of empirical relationships, physically based models or personal judgement (see, e.g., Macedonio and Pareschi, 1992; Iverson, 1997; Iverson *et al.*, 1998; Rickenmann, 1999; Denlinger and Iverson, 2001; Iverson and Denlinger, 2001; Iovine *et al.*, 2003; Iverson, 2003). In many cases, such as at the onset of a crisis, simple hazard models that require a limited number of input parameters and are often empirically based can be particularly valuable (Malin and Sheridan, 1982). In general, the aim of applying simple and/or empirically based models is to obtain a first order approximation of the flow's distal limits with the main advantage of being flexible and able to provide a realistic framework for real-time hazard mitigation. Moreover, simple models can be applied to large areas, providing a preliminary identification of the areas at risk, which could be subjected to more detailed studies.

In the context of empirical modelling of debris flows, the mobility ratio ($\Delta H/L$) can be used for the prediction of the flow's maximum run-out and first-order approximations of the velocity history of debris flows. This is based on the principle that the ratio between the vertical descent of the gravity-driven mass (ΔH) and the corresponding run-out distance (L) can be used to parameterize a friction parameter commonly known as the 'Heim coefficient' (Hsü, 1975; Malin and Sheridan, 1982). This is the 'energy line' concept, originally conceived for rock avalanches by Albert Heim (1882), redefined by Hsü (1975) and further extended to other gravity-driven phenomena such as debris flows (Iverson, 1997), pyroclastic flows (Malin and Sheridan, 1982; Sheridan and Malin, 1983; Hayashi and Self, 1992) and debris avalanches (Siebert, 1984). This mobility index roughly correlates with the volume of the flow (Iverson, 1997), and can be used to approximate the maximum potential run-out of debris flows.

DOI: 10.1002/esp

As regards the inundation area of debris flows, Iverson *et al.* (1998) used scaling analysis to develop equations that predict the maximum cross-sectional and planimetric area as a function of lahar volume. They calibrated these relationships on the basis of 29 lahar paths at nine volcanoes, and implemented them as a set of GIS macros that run within ArcInfo (Schilling, 1998). This procedure enables the automatic mapping of lahar inundation hazard zones (see also Hubbard *et al.*, 1999; Sheridan *et al.*, 1999; Stevens *et al.*, 2003). An approach to evaluate debris flow susceptibility has been proposed by Iovine *et al.* (2003), based on cellular automaton (CA) modelling, which enables the delineation of the areas exposed to the hazardous phenomenon together with its spatial and temporal evolution. Finally, Rickenmann (1999) provides an overview of empirical relationships that can be used to estimate the most important parameters that describe debris flow behaviour such as debris flow peak discharge, mean flow velocity, total travelled distance and run-out distance on the deposition fan.

This paper focuses on the maximum run-out of debris flows. It first characterizes the morphology and presents the volume and mobility, expressed by the Heim coefficient (Hsü, 1975; Malin and Sheridan, 1982; Iverson, 1997), for the events at Sarno (Figure 1). It follows with the calibration of a relationship between the volume and the mobility of these flows. The resulting equation is then embedded into ArcGIS with code written in Visual Basic for Applications (VBA) to allow the automatic production of maps of the maximum extent of debris flows. This code is nested together with another application, which allows the prediction and mapping of the velocity and dynamic pressure of debris flows and which is presented in a companion paper (Toyos *et al.*, 2007). Ultimately, the procedure presented here will contribute towards real-time hazard mitigation and the development of new successful mitigation strategies.

The Study Area

On 5 and 6 May 1998, following two days of intense rains (Onorati *et al.*, 1999) and a particularly wet spring season, volcanic deposits mantling the slopes of the Sarno Mountains (Figure 1) failed and generated several hundred landslides that coalesced and rapidly transformed into debris flows. These events affected the areas of Episcopio and Lavorate and the towns of Quindici, Siano and Bracigliano (Figure 1) (Calcaterra *et al.*, 2000; Pareschi *et al.*, 2002; Crosta and Dal Negro, 2003) as well as the Clanio valley (Pareschi *et al.*, 2002). Landslides began at the heads of gullies (between 700 and 950 m.a.s.l.) at slope angles of more than 33–35°. Following failures, soil slips rapidly transformed into debris flows (Zanchetta *et al.*, 2004) that travelled at speeds of several kilometres per hour (Guadagno *et al.*, 1999) and progressively increased in volume while moving down-slope. Debris flows reached the urban areas and caused more than 150 fatalities and extensive damage to property (Calcaterra *et al.*, 2000; Pareschi *et al.*, 2000; Porfido *et al.*, 2002; Toyos *et al.*, 2003). The economic losses were enormous: more than 50 billion lire were required for the reconstruction of public buildings alone (Caporale, 2000).

The Sarno Mountains are on the margin of the Apennine belt bordered to the Southwest by the Campanian Plain graben and situated 20 km east of the Somma–Vesuvius volcano (Figure 1). They form part of the 'Pizzo d'Alvano' massif, which is composed of Mesozoic–Cenozoic carbonate rocks (Pescatore and Ortolani, 1973) and is mantled with loosely to poorly consolidated volcaniclastic deposits as a result of the eruptive episodes of Mt. Somma–Vesuvius (Calcaterra *et al.*, 2000; Pareschi *et al.*, 2002; Crosta and Dal Negro, 2003). The transition between the hill-slopes and the alluvial plain is marked by two sets of alluvial fans. The oldest of these developed during the late Pleistocene and the youngest, which remains active, during the Holocene (Pareschi *et al.*, 2000; Di Vito *et al.*, 1998). Debris flow deposits dominate the stratigraphy of both sets of alluvial fans (Pareschi *et al.*, 2000; Zanchetta *et al.*, 2004).

Debris Flow Volume

The volume of the flows that affected Episcopio and Lavorate and the morphology of the flows that occurred in the village of Episcopio have been characterized by previous studies (Zanchetta *et al.*, 2004; Oramas Dorta *et al.*, 2006). We refined this analysis and extended it to include the areas of Quindici, Siano and Bracigliano (Figure 1).

Based on the analysis of slope profiles of debris flow paths and on the interpretation of post-event aerial photography we identified a total of 30 flow source areas (Figure 1). The lower limit of these source areas coincides with the apex of the alluvial fan, which was identified by the first large break in slope along the profile. The shape of the deposition areas varied greatly from one flow to another, mainly as a result of natural variations in topography and the density and spatial distribution of infrastructure, which the flows met along their paths.

In many cases, areas within the towns were inundated by more than one event (Figure 1, Table I). Only 10 of the 30 source areas identified evolved into debris flows, which could be recognizable as single events with a clear source, transport and/or deposition area and with no special characteristics (e.g. Ep-2; Table I). For the remaining cases, we

DOI: 10.1002/esp

Table I. Morphological characterization of the debris flows in the study area

Source	Special features	Event	Morphology
Ep-1	–	Ep-1	S
Ep-2	–	Ep-2	S
Ep-3a	Merges with Ep-3b at deposition	Ep-3	C
Ep-3b	Merges with Ep-3a at deposition		
Ep-4	Flow diverges into two channels near the source area, which then merge again before deposition	Ep-4	C
Ep-5	–	Ep-5	S
Ep-6a	Merges with Ep-6b	Ep-6	C
Ep-6b	Merges with Ep-6a and Ep-7a channel joins them		
Ep-7a	Narrow channel that merges with Ep-6b. Deposition area is not distinguishable	Ep-7a	C
Ep-$7b_1$	Merges at transport with Ep-$7b_2$	Ep-7	C
Ep-$7b_2$	Merges at transport with Ep-$7b_1$		
Lav-1	–	Lav-1	S
Lav-2a	Merges with Lav-2b and Lav-2c and then converges with Lav-2d	Lav-2	C
Lav-2b	Merges with Lav-2a and Lav-2c, and with Lav-2d further downstream		
Lav-2c	Merges with Lav-2a and Lav-2b, and with Lav-2d further downstream		
Lav-2d	Some material diverges and deposits before joining the material coming from the other three source areas		
Sia-1	–	Sia-1	S
Sia-2a	Merges with Sia-2b	Sia-2	C
Sia-2b	Merges with Sia-2a		
Brac-1a	Merges with transport zone of Brac-1b	Brac-1	C
Brac-1b	Merges with Brac-1a (as Ep-7a with Ep-6b)		
Quin-1a	Transport zone merges with source area of Quin-1b	Quin-1	C
Quin-1b	Source area receives material from Quin-1a. Deposition area is not visible. Material flowed into a channel that passes north of the town of Quindici		
Quin-2	–	Quin-2	S
Quin-3	–	Quin-3	S
Quin-4a	Merges with Quin-4b	Quin-4	C
Quin-4b	Merges with Quin-4a		
Quin-5	–	Quin-5	S
Quin-6	–	Quin-6	S
Quin-7	–	Quin-7	S

The first column contains the 30 source areas originally identified. The column *Event* assumes that indistinguishable transport and/or deposition areas resulting from more than one source area correspond to one single event (e.g. Lav-2). The last column indicates a complex morphology (C) for these flows and simple morphology (S) for those with a clear and single source, transport and/or deposition area (e.g. Ep-2). Quin-1 and Ep-7a were excluded from further consideration, since deposition areas were not distinguishable.

assumed indistinguishable transport zones and/or deposition areas of debris flows resulting from more than one source to correspond to single events (e.g. Lav-2, Ep-6; Table I). From now on we refer to the events belonging to the first and second groups (Figure 1, Table I) as flows with *simple* and a *complex* morphology, respectively.

In the source areas (Figure 1) the thickness of the scarps left by the initial landslides varied between 0·5 and 2 m (Pareschi *et al.*, 2000, 2002; Zanchetta *et al.*, 2004). Thus, we based the volume calculations on an average depth of scarps of 1·2 m and on the basis of the range 0·5–2·0 m; we also computed volume uncertainty ranges, which represent a bracket of +/–60%. The reported scarp depths are the best estimates available based on fieldwork, detailed geologic and geomorphologic analysis and air photo interpretation (Pareschi *et al.*, 2000, 2002; Zanchetta *et al.*, 2004).

Volumes in Table II represent the maximum amount of material that collapsed within the perimeters of the source areas. The magnitudes of those events with a complex morphology (Table I) are the result of adding the volumes of the contributing source areas. While these assumptions may lead to overestimates we justify this, in part, by considering these estimates as worst-case scenarios for each debris flow event. We assumed the progressive increase in volume along transport zones on the alluvial fan surface to be negligible (Zanchetta *et al.*, 2004). While this bulking process

DOI: 10.1002/esp

Table II. Debris flow volumes based on the average scarp thickness and limits of uncertainty, vertical descent (ΔH) in metres, distance run-out (L) in km, mobility ratios ($\Delta H/L$) and depression angles (θ) in degrees (°)

	Volumes (m^3) for thicknesses of										
Basin/event	**1·2 m**	**0·5 m**	**2 m**	ΔH_1*	L_1*	$\Delta H/L_1$*	θ_1*	ΔH_2**	L_2**	$\Delta H/L_2$**	θ_2**
Ep-1	$1{\cdot}6 \times 10^4$	$6{\cdot}5 \times 10^3$	$2{\cdot}6 \times 10^4$	290	1·15	0·25	14·2	560	1·51	0·37	20·3
Ep-2	$1{\cdot}1 \times 10^5$	$4{\cdot}8 \times 10^4$	$1{\cdot}9 \times 10^5$	140	1·11	0·13	7·3	660	1·94	0·34	18·9
Ep-3	$1{\cdot}7 \times 10^5$	$6{\cdot}9 \times 10^4$	$2{\cdot}8 \times 10^5$	120	0·97	0·12	7·0	650	1·83	0·36	19·6
Ep-4	$4{\cdot}5 \times 10^4$	$1{\cdot}9 \times 10^4$	$7{\cdot}5 \times 10^4$	150	0·86	0·18	10·2	690	1·71	0·40	21·9
Ep-5	$1{\cdot}2 \times 10^5$	$5{\cdot}0 \times 10^4$	$2{\cdot}0 \times 10^5$	250	1·69	0·15	8·4	800	2·72	0·29	16·4
Ep-6	$1{\cdot}7 \times 10^5$	$7{\cdot}2 \times 10^4$	$2{\cdot}9 \times 10^5$	230	1·77	0·13	7·2	770	2·68	0·29	16·1
Ep-7	$1{\cdot}3 \times 10^5$	$5{\cdot}6 \times 10^4$	$2{\cdot}2 \times 10^5$	280	1·87	0·15	8·6	840	2·75	0·30	16·9
Lav-1	$1{\cdot}3 \times 10^5$	$5{\cdot}3 \times 10^4$	$2{\cdot}1 \times 10^5$	250	2·14	0·12	6·7	900	3·25	0·28	15·4
Lav-2	$2{\cdot}5 \times 10^5$	$1{\cdot}0 \times 10^5$	$4{\cdot}1 \times 10^5$	210	1·99	0·11	6·0	860	3·22	0·27	15·0
Quin-2	$4{\cdot}7 \times 10^4$	$2{\cdot}0 \times 10^4$	$7{\cdot}8 \times 10^4$	240	1·29	0·19	10·6	670	1·94	0·34	18·9
Quin-3	$2{\cdot}0 \times 10^4$	$8{\cdot}5 \times 10^3$	$3{\cdot}4 \times 10^4$	230	0·86	0·27	15·0	530	1·34	0·39	21·5
Quin-4	$6{\cdot}4 \times 10^4$	$2{\cdot}7 \times 10^4$	$1{\cdot}1 \times 10^5$	250	0·99	0·25	14·1	560	1·61	0·35	19·2
Quin-5	$1{\cdot}2 \times 10^4$	$4{\cdot}8 \times 10^3$	$1{\cdot}9 \times 10^4$	90	0·47	0·19	11·0	240	0·69	0·35	19·3
Quin-6	$3{\cdot}2 \times 10^4$	$1{\cdot}3 \times 10^4$	$5{\cdot}3 \times 10^4$	210	1·26	0·16	9·2	550	1·90	0·29	16·1
Quin-7	$8{\cdot}5 \times 10^4$	$3{\cdot}6 \times 10^4$	$1{\cdot}4 \times 10^5$	80	0·89	0·09	5·3	660	2·51	0·26	14·7
Brac-1	$1{\cdot}6 \times 10^5$	$6{\cdot}9 \times 10^4$	$2{\cdot}7 \times 10^5$	150	1·47	0·10	5·9	580	2·38	0·24	13·7
Sia-1	$1{\cdot}7 \times 10^4$	$7{\cdot}0 \times 10^3$	$2{\cdot}8 \times 10^4$	150	0·67	0·23	12·9	450	1·11	0·41	22·2
Sia-2	$6{\cdot}4 \times 10^4$	$2{\cdot}7 \times 10^4$	$1{\cdot}1 \times 10^5$	180	1·02	0·18	10·1	480	1·45	0·33	18·4

* ΔH_1, L_1, $\Delta H/L_1$ and θ_1 correspond to energy lines starting at the apex of the alluvial fan.
** ΔH_2, L_2, $\Delta H/L_2$ and θ_2 correspond to energy lines starting at the top of the scarp.

(Pierson, 1995; Iverson, 1997) has been documented on the alluvial fans, the increase in volume was not significant, since the run-out distances were rather short, at most 2·1 km from the apex of the alluvial fan of Lav-1 (Figure 1).

A total of $1{\cdot}8 \times 10^6$ m^3 of material was removed from the hill slopes in the area. A maximum of $1{\cdot}3 \times 10^5$ m^3 was estimated at Lav-1, a minimum of $1{\cdot}2 \times 10^4$ m^3 at Quin-5 and a typical value of $5{\cdot}7 \times 10^4$ m^3 (Figure 1, Table II). These debris flows can be considered of small to moderate size compared with event magnitudes recorded elsewhere (Iverson, 1997; Iverson *et al.*, 1998) and are in agreement with previous estimates in the area (de Riso *et al.*, 1999; Zanchetta *et al.*, 2004; Oramas Dorta *et al.*, 2006).

Debris Flow Mobility ($\Delta H/L$)

The ratio between the drop in height (ΔH) and the horizontal run-out (L) of flows, as measured between the source and deposition areas, illustrates the mobility of gravity-driven mass flows. These two points define an energy line and the dynamic properties of the flow mass are constrained by the tangent of the slope angle of this line relative to the horizontal (Malin and Sheridan, 1982; Hayashi and Self, 1992) (Figure 2). This dimensionless parameter represents the flow's resistance due to friction and incorporates the effects of internal forces but also depends on external forces that act at the bed to convert gravitational energy into horizontal motion (Iverson, 1997). This relationship ($\mu = \Delta H/L$) is, in theory, mass independent (Iverson, 1997; Hayashi and Self, 1992), and both ΔH and L are strictly defined by lines that connect the centres of mass of the flow's source and deposition areas. For practical reasons, the energy line is usually drawn between the upper and lower limits of the flow (Iverson, 1997).

The conceptual model applies to a single event, whereas the events at Sarno were the result of the coalescence of many landslides. This complicated substantially the identification of the starting point for the energy lines and was even more problematic with the flows of complex morphology (i.e. where the volume is the result of more than one source area). Therefore, in order to investigate possible simple approximations of the centres of mass of the flows, we distinguished two types of mobility: (i) on the basis of an energy line starting at the highest location of the landslide scar of the source area and (ii) based on an energy line that connects the apex of the alluvial fan with the distal limit of the flow. The first type represents the maximum potential energy available for the conversion of gravitational energy into horizontal motion and for forcing the flow to stop. The second one represents the energy line of completely developed debris flows, since it is at the apex of the alluvial fan, where we are able to ascertain that the

DOI: 10.1002/esp

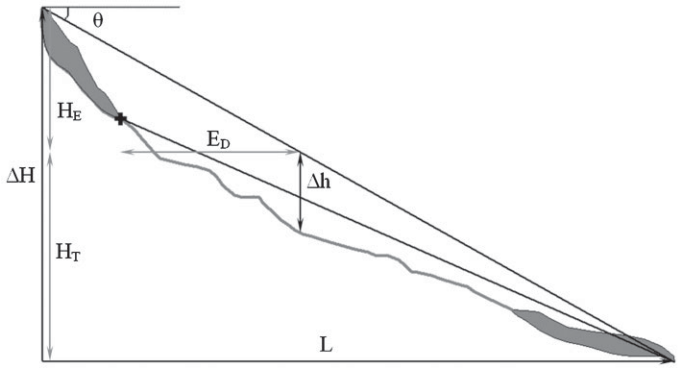

Figure 2. Diagram illustrating the principle of the energy line (Hsü, 1975). The mobility ratio ($\Delta H/L$) is defined by the drop in height (ΔH) over the distance run-out (L) and the energy line forms a depression angle (θ) with the horizontal. Two energy lines are shown, one starting from the highest landslide scar at the top of the source area and the other one referenced from the alluvial fan apex (i.e. the black cross). This diagram also shows the parameters used by the algorithm to derive maximum run-out within ArcGis, i.e. E_D = Euclidean distance from the apex of the alluvial fan, $H_E = E_D\ \Delta H/L$, ΔH = DEM elevation + user-defined altitude above the starting point, H_T (energy cone elevation) = $\Delta H - H_E$, $\Delta h = H_T$ – DEM elevation. If $\Delta h > 0$ then the cell has a value of 1, otherwise it has a value of 0. All distances and elevations are measured in metres.

final volume of the flow formed as a consequence of the coalescence of the initial landslides. For this reason, although this location excludes the source area, it is considerably closer to the centre of mass of the source volume than the top of the scarp. The statistical analysis provides insights in these respects (see next section).

The mobility of the Sarno flows based on the apex of the alluvial fan ranged from 0·27 to 0·09 (Table II), equivalent to depression angles between 15 and 5·3°. The mobility indices based on the top of the scarp were higher (Table II). This latter range of mobility ratios falls within that quoted by Iverson (1997) for debris flows less than 10^5 m^3, which would apply to the volumes observed in the Sarno area (Table II). Both sets of calculations define mobility envelopes with the ones based on the apex of the alluvial fan representing the maximum and the ones based on the scarp the minimum mobility.

Statistical Analysis

We analysed the relationship between volume and mobility (Figure 3) by performing regression analyses with data from the 18 debris flows summarized in Table II and with data from the 10 flows of simple morphology (Tables I and II). The statistical fits were good (Table III) when we used mobility ratios based on an energy line starting at the apex of the alluvial fan (Figure 3). When we used mobility indices calculated on the basis of energy lines starting at the top of the scarp, the fits were rather poor (Figure 3, Table III). The lognormal relationships were stronger (Table III) when we used the 10 flows with a simple morphology (Table I).

According to previous research, Corominas (1996) observed that all types of landslides increase in mobility with an increase in flow volume and that this relationship starts from the smallest magnitudes. Iverson (1997), however, quoted that debris flows with $V > 10^5$ m^3 appear to increase in mobility in proportion to the logarithm of the volume, while for smaller events the mobility ratio remains fixed at ~0·25–0·5. Both used measures of mobility based on energy lines starting at the head of the source areas and our results obtained for the mobilities based on the top of the scarp (Table III, Figure 3) are in agreement with what was quoted by Iverson (1997). We attributed these contrasts to the size, distribution and origin of the data. Corominas's (1996) dataset was large ($n = 71$) and well constrained and included mostly rain-triggered events. The volumes spanned various orders of magnitude but most of them were less than or equal to 10^4 m^3, a few of the order of 10^4–10^5 m^3 and some greater than or equal to 10^6 m^3. Iverson's (1997) observations, on the other hand, were based on debris flows of various origins and flow path geometries. The volume data spanned various orders of magnitude (10^1–10^9 m^3) and only five out of twelve volumes were less than or equal to 10^5 m^3. Our data were very well constrained, and while the size of the dataset compared to Iverson's (1997), the volumes we used were 10^4–10^5 m^3, i.e. orders of magnitude that were unrepresented in both Corominas's (1996) and Iverson's (1997) studies. These contrasts may be reflecting an effect of scale, in the sense that the volume and mobility of debris flows correlate well only when the datasets span various orders of magnitude, or may be showing that the datasets were not sufficiently large and well distributed. To expand on these issues future investigations will require a

DOI: 10.1002/esp

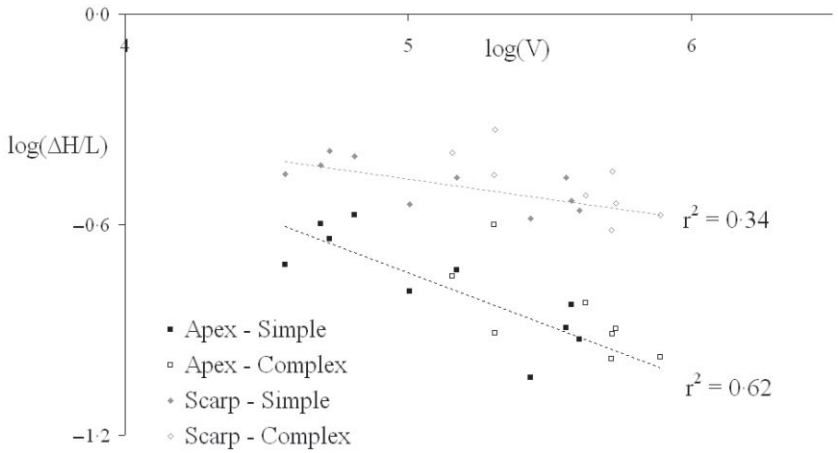

Figure 3. Debris flow mobility (m m^{-1}) versus volume (m^3) and statistical fits of the calibrations. The data shown is discriminated in terms of both the starting location of the energy line (i.e. apex and scarp) and the classification of morphologies (simple and complex). The regression line equation in exponential form for the mobility based on energy lines starting at the top of the scarp is $\Delta H/L = 1{\cdot}12V^{-0{\cdot}11}$ and at the apex of the alluvial fan $\Delta H/L = 3{\cdot}31V^{-0{\cdot}28}$.

large number of observations for single orders of magnitude and datasets will have to be strictly stratified in terms of triggering mechanisms, confinement, morphology and the presence of natural or man-made obstructions, among other factors. Corominas's (1996) work constituted an important step in these respects and an important point is that the coefficients of the log-normal relationships he obtained for debris flows were very close to ours (Table III). This supports the hypothesis that datasets are not sufficiently large and well distributed. We must recall that while the r^2 (0·34) for the energy lines based on the top the scarp was low, the regression was statistically significant ($p < 0{\cdot}05$, Table III).

Finally, the significant contribution of our results is given by the strong correlation observed between the volume and the mobility based on the apex of the alluvial fan. These results provide quantitative support to the hypothesis that apex of the alluvial fan approximates the location of the centre of mass of the source volume of the flow better than the top of the scarp, since at the apex that the flow is mature and complete. Moreover, these results provide the basis for a practical solution for hazard mapping, since it is easier to identify the apex of the alluvial fan for hazard mapping of future debris flow events than the top of the scarp of potential source areas. On the other hand, the good statistical fits obtained (Table III) may also reflect the specific geomorphic setting of the studied events and the good constraints on the source, transport and/or deposition areas. The larger r^2 values observed for the flows of simple morphology ($n = 10$) may also indicate an effect of the quality of the delineation of the events on the statistical calibration.

Table III. Regression results for log(V) and log($\Delta H/L$) based on energy lines starting at the apex of the alluvial fan ($\Delta H/L_1$) and at the highest landslide scars ($\Delta H/L_2$). Results are also included for the 10 flows with a simple morphology (Table I).

	All ($n = 18$)		**Simple morphology ($n = 10$)**	
	($\Delta H/L_1$)	**($\Delta H/L_2$)**	**($\Delta H/L_1$)**	**($\Delta H/L_2$)**
Equation	$\Delta H/L = 3{\cdot}31V^{-0{\cdot}28}$*	$\Delta H/L = 1{\cdot}12V^{-0{\cdot}11}$	$\Delta H/L = 4{\cdot}27V^{-0{\cdot}30}$	$\Delta H/L = 1{\cdot}12V^{-0{\cdot}11}$
r^2	0·62	0·34	0·67	0·41
Standard error	0·09	0·07	0·09	0·06
p	<0·01	<0·05	<0·01	<0·05
Slope	−0·28	−0·11	−0·30	−0·11
Lower 95% slope	−0·39	−0·19	−0·46	−0·22
Upper 95% slope	−0·16	−0·03	−0·14	−0·01
Intercept	0·52	0·05	0·63	0·05
Lower 95% intercept	−0·04	−0·35	−0·12	−0·43
Upper 95% intercept	1·07	0·44	1·38	0·53

* The equation obtained for the mobilities based on energy lines starting at the apex of the alluvial fan was the one implemented within a GIS environment. The constant of proportionality of all equations results from calculating the antilogarithm of the intercept of the log-normal relationships.

DOI: 10.1002/esp

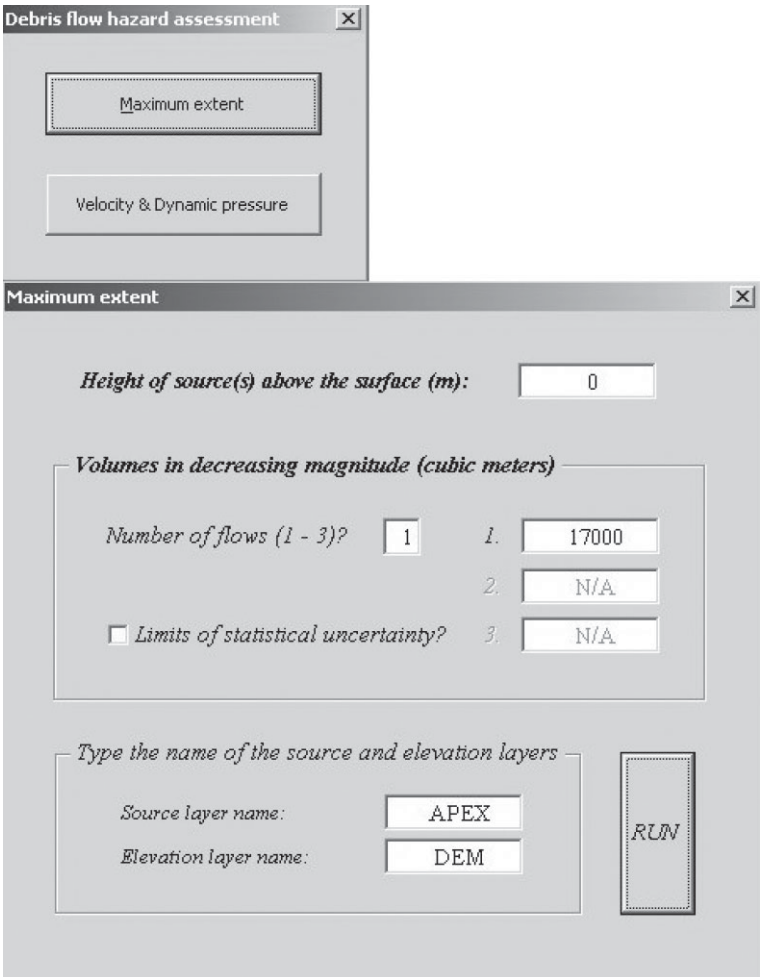

Figure 4. Graphic user interface for the inputs to simulate debris flow maximum extent.

Implementation

We implemented the equation $\Delta H/L = 3{\cdot}29V^{-0{\cdot}28}$ developed on the basis of the 18 debris flow volumes and mobilities assuming the energy line starting at the apex of the alluvial fan (Table III) with code written in VBA that runs within ArcGIS and is deployed as a template from which any ArcGIS project can be derived. The graphic user interface (GUI) (Figure 4) requires (i) up to three volumes, (ii) the height above the ground surface at the apex of the alluvial fan and (iii) the names of a vector point layer with the location of the starting point of the flow and of a raster layer with elevation data (DEM). For each user-selected volume, the code calculates the $\Delta H/L$ and then searches the intersection between the energy line and the ground surface through the implementation of an algorithm, which can be summarized as follows (Figure 2).

I. Find Euclidean distances from the starting point (E_D) (i.e. apex of the alluvial fan).
II. Multiply E_D by $\Delta H/L$ in order to calculate H_E.
III. Extract from the DEM the elevation at the starting point location and add it to the altitude defined by the user (Figure 5) to obtain ΔH.
IV. Subtract H_E (step II) from ΔH (step III) to calculate the energy line elevation, H_T.
V. Subtract the surface elevation from the energy line elevation (H_T) to calculate Δh. If $\Delta h > 0$ then the cell is within, while if $\Delta h < 0$ then it is beyond, the distal limits of the flow. The code assigns a value of 1 to the first group of cells and a value of 0 to the latter.

DOI: 10.1002/esp

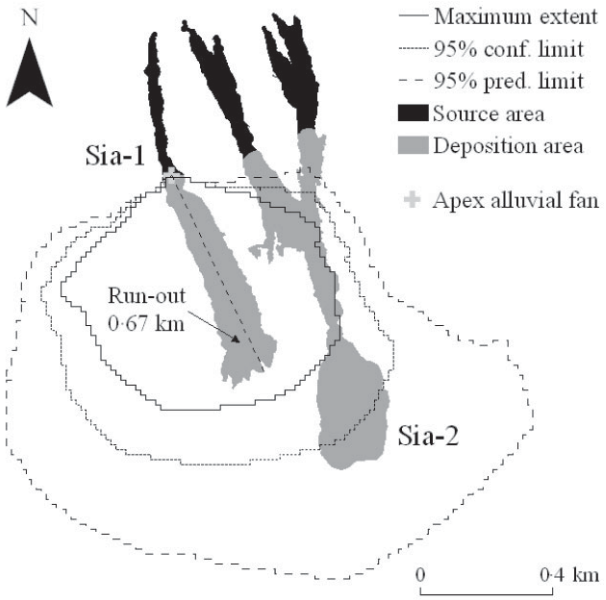

Figure 5. Actual source and deposition areas of Sia-1 and maximum extent given by the mobility at the regression line, and the maximum confidence and prediction limits, for the $1{\cdot}7 \times 10^4$ m^3 measured in Sia-1 (Table II), starting at the apex of the alluvial fan. Predicted run-outs are defined by the intersection between the graphic output and the stream of interest.

The output is a vector layer with the maximum potential limit of the flow starting at the apex of the alluvial fan (Figure 5). If there is more than one user-selected volume, then the code generates as many output layers as the number of input volumes selected. The checkbox *Limits of uncertainty* (Figure 4) allows the delineation of the maximum predicted extent according to the 95% confidence and prediction limits of the regression model (Figure 5). In this case, the program generates three vector layers, one for the maximum extent given by the mobility index at the regression line and the other two for the 95% confidence and prediction limits of the regression model (Figure 5). Finally, multiple source simulations of the same flow are also possible. The user obtains a grid with percentage probabilities ranging between 0 and 100% and a vector dataset of maximum extent that refers to the last starting point in the attribute table, as in the simulations with only one starting point (Figure 5). Thus, this approach enables the incorporation of uncertainties in the identification of the apex of the alluvial fan into the hazard mapping process. This kind of information provides the opportunity to incorporate safety margins into hazard maps.

Sensitivity Analysis

We evaluated the effects of uncertainties in the input volume estimates on the statistical calibration and on the run-out predictions by the computer application. We also examined the departures from the run-outs given by the mobilities at the regression line according to the 95% confidence and prediction limits of the regression model. For the first task, we performed regression analysis again but with volumes estimates based on 0·5 and 2 m thickness of the scarp (Table II). For the latter two, we performed simulations of those events with a simple morphology ($n = 10$, Table I) on DEMs derived from 1:25 000 scale topographic maps. We used two types of misfit function: (a) the average misfit (%) ($\Sigma[(L_a - L_p) \times 100/L_a]_i/n$) and (b) the root mean square error (RMSE = $[\Sigma(L_a - L_p)^2/n]^{1/2}$), where L_a is the actual run-out of the flow, L_p is the flow run-out distance predicted by the equation and n is the number of observations.

The aim here is to provide a first order approximation to potential users of the effects of the main sources of uncertainty on the approach presented for their eventual incorporation of additional safety margins into the hazard mapping process. For this reason, we used volume uncertainty limits based on extreme values of the scarp heights but being aware that a complete sensitivity analysis would involve at least the simulation of random variation of individual volume estimates. More detailed studies in the future will need to incorporate this variation into the statistical calibration and the GIS implementation.

DOI: 10.1002/esp

Table IV. Regression results with volumes based on the average scarp thickness and limits of uncertainty

Thickness (m)	0·5	1·2	2
r^2	0·62	0·62	0·62
Standard error	0·09	0·09	0·09
p	<0·01	<0·01	<0·01
Intercept	0·41	0·52	0·58
Lower 95% intercept	−0·10	−0·04	−0·005
Upper 95% intercept	0·93	1·07	1·16
Slope	−0·28	−0·28	−0·28
Lower 95% slope	−0·39	−0·39	−0·39
Upper 95% slope	−0·16	−0·16	−0·16

Sensitivity of the statistical calibration

As a first order approximation we calibrated the equations again with volumes based on the uncertainty limits of the thickness of the scarp. Our results showed that the r^2, standard errors and levels of significance of the different regression models were identical. The slopes of the regression lines as well as the confidence intervals of the coefficients of the different regression models were also identical. Intercepts were very similar and statistically indistinguishable (Table IV).

The uncertainty limit established and applied to each volume is constant, and thus it is reasonable to expect the same slope but different intercepts. The largest intercept resulted from the calibration with the volumes based on the maximum scarp thickness, followed by the one based on volumes calculated on the basis of the average thickness and finally by the calibrated coefficient based on the minimum volumes (Table IV). Thus, it would be reasonable to consider an intercept range of 0·41–0·58 in order to account for the uncertainty in the regression line coefficients derived from the consideration of the uncertainty limits in the input volume estimates.

Sensitivity of the automatic procedure

The regression line coefficients were insensitive to considered uncertainties in flow input volumes as per the 0·5–2·0 m observed scarp thickness range. Therefore, this section follows with an analysis of the effects of uncertainties in the input volumes on the equation based on the average thickness, i.e. the equation implemented by the computer application: $\Delta H/L = 3{\cdot}29V^{-0{\cdot}28}$.

The average misfit between the actual and predicted run-outs resulted in ~30% for volumes based on both limits of uncertainty of scarp thickness, while it was ~20% for volumes based on the average thickness of the scarps. Root mean square errors were 0·4, 0·2 and 0·4 km for the minimum, average and maximum scarp thickness, respectively. The variation in thickness within the range 0·5–2 m represents an uncertainty of +/–60% in the volumes used in the statistical calibration. Given the large size of the uncertainty applied to the volume estimates, the misfits in the run-out predictions by this approach would rarely exceed in reality the +/–30% obtained from our calculations (see above). Therefore, we consider that a misfit of ~30% is realistic and should be used as a limit of uncertainty to express model results, in order to cover for potential errors in the input volumes. Alternatively, this precision may be expressed in distance units with an RMSE of +/–0·4 km. For instance, the model simulates a run-out of 1·2 km for the $1{\cdot}1 \times 10^5$ m^3 debris flow in Ep-2, which is within 0·8 and 1·6 km from the source, given an uncertainty of ~60% in the input magnitude selected.

Statistical uncertainties

The 95% confidence and prediction limits of simulations performed with the volumes of the 10 'simple' flows (Tables I and II) were, on average, 25 and 85% longer than the run-outs given by the mobilities at the regression line, respectively. Root mean square differences for both limits of statistical uncertainty were 0·3 and 0·9 km, respectively. These misfits are to provide an idea of the departure of these limits of uncertainty from the value of the mobility predicted at the regression line. Depending on whether the user wishes to cover for the uncertainty around the mean response and/or the actual mobilities used in the statistical calibration for a specific debris flow volume, the user may use the option provided by the computer application to simulate the maximum extent and resulting run-out that corresponds to the confidence and prediction limits of the regression model, respectively.

DOI: 10.1002/esp

Conclusions

We have presented a simple approach for the rapid and objective prediction and delineation of small volume debris flow run-outs with an associated uncertainty of ~0·2 km (20%). However, model verification is needed before extending this to larger events and other geomorphic settings.

We were able to calibrate a relationship between the volume and mobility of small debris flows, which appear to correlate well when the mobility is based on energy lines referenced from the apex of the alluvial fan. Thus, it seems that the fan apex approximates the centre of mass of the source volume of small rain-triggered debris flows generated by the coalescence of multiple landslides better than the top of the scarp, probably because at the fan apex the flow is mature and complete. Moreover, the identification of the apex of the alluvial fan for modelling hazards of future events is more straightforward than the identification of the top of the scarp of potential source areas, since the latter involves more uncertainty. More data for specific orders of magnitude are required to confirm whether a relationship holds between the flow volume and mobility based on energy lines referenced from the head of the source area. Besides, the success of the statistical calibration was also determined by the adequate delineation of the source, transport and/or deposition areas, which was possible thanks to the good quality of the data sources. This could be confirmed by the larger statistical fits obtained with the data on the flows with a simple morphology. In fact, the effects of flow morphology as well as of other factors such as the topography of the fan, the level of flow confinement (e.g. channelled versus open-fan flows) and the presence of natural and man-made obstructions on run-out predictions are interesting issues to be addressed by future investigations. The work carried out by Corominas (1996) constitutes an important step in these respects.

The approach presented allows the user to simulate and incorporate safety margins for flow run-out prediction, which would account for uncertainties in the input volume estimates and in the location of the starting point for the flow, and statistical uncertainties given by the confidence and prediction limits of the regression model. First, the effects of errors in the input volume estimates suggest that an appropriate horizontal resolution for the resulting hazard maps should not exceed 0·4 km along the stream of interest. Second, the possibility of multiple starting point simulations allows the investigation of the effects of the topography that surrounds the apex of the alluvial fan. Finally, the ability of the code to predict and delineate the maximum potential run-outs according to the confidence and prediction limits of the regression model provides users, managers and decision makers with the opportunity to decide on additional safety margins for hazard assessment. The software is available upon request and we expect to make it public in ESRI's website in the near future.

Acknowledgements

This research constitutes a portion of the work carried out by the first author towards the PhD degree at the University of Cambridge, UK, which was funded and supported by Fundación YPF—Argentina, the Department of Geography of Cambridge University, King's College Cambridge and the Cambridge Overseas Trust. We also thank the Italian National Research Council (CNR), the Italian Institute of Geophysics and Volcanology (INGV), the University of Pisa (Italy) and the Vesuvian Observatory for providing funding, data and support in the field. Thanks very much also to the three anonymous reviewers of the manuscript, who contributed towards a substantial improvement of this article.

References

Calcaterra D, Parise M, Palma B, Pelella L. 2000. Multiple debris-flows in volcaniclastic materials mantling carbonate slopes. *Proceedings of the Second International Conference on Debris-Flow Hazards Mitigation: Mechanics, Prediction and Assessment*. Balkema: Taipei, Taiwan; 99–107.

Caporale R. 2000. *The May 1998 Landslides in the Sarno Area in Southern Italy: Rethinking Disaster Theory*, Quick Response Report 131, University of Colorado.

Corominas J. 1996. The angle of reach as a mobility index for small and large landslides. *Canadian Geotechnical Journal* **33**: 260–271.

Crosta GB, Dal Negro PD. 2003. Observations and modelling of soil slip-debris flow initiation processes in pyroclastic deposits: the Sarno 1998 event. *Natural Hazards and Earth System Sciences* **3**: 53–69.

de Riso R, Budetta P, Calcaterra D, Santo A. 1999. Le colate rapide in terreni piroclastici del territorio campano. *Atti del Convengo Previsione e Prevenzione di Movimenti Franosi Rapidi*, Trento, Italy; 133–150 (in Italian).

Denlinger RP, Iverson RM. 2001. Flow of variably fluidised granular masses across three-dimensional terrain 2. Numerical predictions and experimental tests. *Journal of Geophysical Research* **106**(B1): 553–566.

Di Vito MA, Sulpizio R, Zanchetta, G. 1998. I depositi ghiaiosi della valle dei Torrenti Clanio e Acqualonga (Campania Centro-Orientale): significato stratigrafico e ricostruzione paleoambientale. *Quaternario* **11**: 273–286 (in Italian).

Guadagno FM, Celico PB, Esposito L, Perriello Zampelli S, Piscopo V, Scarascia-Mugnozza G. 1999. The debris flows of 5–6 May 1998 in Campania, Southern Italy. *Landslide News* **12**: 5–7.

Hayashi JN, Self S. 1992. A comparison of pyroclastic flow and debris avalanche mobility. *Journal of Geophysical Research* **97**(B6): 9063–9071.

Heim A. 1882. *Zeitschrift der Deutschen Geologischen Gesellschaft* **34**: 74; *Bergsturz und Menschenleben* (Zürich, 1932) (in German).

Hsü J. 1975. Catastrophic debris streams (sturzstroms) generated by rockfalls. *Geological Society of America Bulletin* **86**: 129–140.

Hubbard BE, Sheridan M, Carrasco-Nuñez G, Scott KM 1999. Application of a GIS model for predicting the impact of medium to large debris flows from Pico de Orizaba (Citlaltepetl), Mexico. *EOS Transaction AGU Fall Meeting* **80**(46).

Iovine G, Di Gregorio S, Lupiano V. 2003. Assessing debris flow susceptibility. In *Proceedings of the Third International Conference on Debris-Flow Hazards Mitigation: Mechanics, Prediction and Assessment*, Vol. 1, Rickenmann D, Cheng-lung C (eds). Millpress: Rotterdam, Netherlands: 623–634.

Iverson RM. 1997. The physics of debris flows. *Reviews of Geophysics* **35**: 245–296.

Iverson RM. 2003. The debris flow rheology myth. In *Proceedings of the Third International Conference on Debris-Flow Hazards Mitigation: Mechanics, Prediction and Assessment*, Vol. 1, Rickenmann D, Cheng-lung C (eds). Millpress: Rotterdam, Netherlands: 303–314.

Iverson RM, Denlinger RP. 2001. Flow of variably fluidised granular masses across three-dimensional terrain: 1. Coulomb mixture theory. *Journal of Geophysical Research* **106**(B1): 537–552.

Iverson RM, Schilling SP, Vallance JW. 1998. Objective delineation of lahar-inundation hazard zones. *Geological Society of America Bulletin* **110**(8): 972–984.

Macedonio G, Pareschi MT. 1992. Numerical simulation of some lahars from Mount St. Helens. *Journal of Volcanology and Geothermal Research* **54**: 65–80.

Malin MC, Sheridan MF. 1982. Computer-assisted mapping of pyroclastic surges. *Science* **217**: 637–640.

Onorati G, Braca G, Iritano G. 1999. Evento idrogelogico del 4, 5 e 6 maggio 1998 in Campania. Monitoraggio e analisi idrologica. *Atti della Accademia Nazionale dei Lincei* **154**: 103–108 (in Italian).

Oramas Dorta D, Toyos G, Oppenheimer C, Pareschi MT, Sulpizio R, Zanchetta G. 2006. Empirical modelling of the 1998 small debris flows in Sarno (Italy) using LAHARZ. *Natural Hazards*. DOI: 10.1007/s11069-006-0035-5

Pareschi MT, Favalli M, Giannini F, Sulpizio R, Zanchetta G, Santacroce R. 2000. May 5, 1998, debris flows in circumvesuvian areas (Southern Italy): insights for hazard assessment. *Geology* **7**: 629–642.

Pareschi MT, Santacroce R, Sulpizio R, Zanchetta G. 2002. Volcaniclastic debris flows in the Clanio Valley (Campania, Italy): insights for the assessment of the hazard potential. *Geomorphology* **43**: 219–231.

Pescatore T, Ortolani F. 1973. Shema tettonico dell'Appennino campano-lucano. *Bollettino Societa Geologica Italiana* **92**: 453–473 (in Italian).

Pierson TC. 1995. Flow characteristics of large eruption-triggered debris flows at snow-clad volcanoes: constrains for debris-flow models. *Journal of Volcanology and Geothermal Research* **66**: 283–294.

Porfido S, Esposito E, Alaia F, Esposito G, Laccarino G. 2002. Ill dissesto idrogeologico: inventario e prospettive. *Atti della Accademia Nazionale dei Lincei* **181**: 457–466.

Rickenmann D. 1999. Empirical relationships for debris flows. *Natural Hazards* **19**: 47–77.

Schilling SP. 1998. *LAHARZ: GIS Programs for Automated Delineation of Lahar-Hazard Zones*, US Geological Survey Open-File Report 98-638.

Sheridan M, Hubbard BE, Hooper DM, Abrams M. 1999. Hazard zones outlining inundation limits for debris flows and debris avalanches at Volcán Colima, Mexico. *EOS Transaction AGU Fall Meeting* **80**(46).

Sheridan M, Malin M. 1983. Application of computer-assisted mapping to volcanic hazard evaluation of surge eruptions: Vulcano, Lipari. *Journal of Volcanology and Geothermal Research* **17**: 187–202.

Siebert L. 1984. Large volcanic debris avalanches: characteristics of source areas, deposits and associated eruptions. *Journal of Volcanology and Geothermal Research* **22**: 163–197.

Smith GA, Lowe DR. 1991. Lahars: volcano–hydrologic events and deposition in the debris flow–hyperconcentrated flow continuum. *Sedimentation in Volcanic Settings, SEPM Special Publication* **45**: 59–69.

Stevens NF, Manville V, Heron DW. 2003. The sensitivity of a volcanic flow model to digital elevation model accuracy: experiments with digitised map contours and interferometric SAR at Ruapehu and Taranaki volcanoes, New Zealand. *Journal of Volcanology and Geothermal Research* **119**: 89–105.

Toyos G, Gunasekera R, Oppenheimer C, Pareschi MT, Sulpizio R, Zanchetta G. 2007. GIS-assisted modelling for debris flow hazard assessment based on the events of May 1998 in the area of Sarno, Southern Italy: II. Velocity and dynamic pressure. *Earth Surface Processes and Landforms* under review.

Toyos G, Oppenheimer C, Pareschi MT, Sulpizio R, Zanchetta G, Zuccaro G. 2003. Building damage by debris flows in the Sarno area, Southern Italy. In *Proceedings of the Third International Conference on Debris-Flow Hazards Mitigation: Mechanics, Prediction and Assessment*, Vol. 2, Rickenmann D, Cheng-lung C (eds). Millpress: Rotterdam, Netherlands: 1209–1220.

Zanchetta G, Sulpizio R, Pareschi MT, Leoni FM, Santacroce R. 2004. Characteristics of May 5–6, 1998 volcaniclastic debris-flows in the Sarno area of Campania, Southern Italy: relationships to structural damage and hazard zonation. *Journal of Volcanology and Geothermal Research* **133**: 377–393.

DOI: 10.1002/esp